

# APRA Proposal: Large Balloon Reflector (LBR)

Submitted by:  
Prof. Christopher Walker  
University of Arizona  
888 N. Euclid Ave  
Tucson, AZ 85719-4824

## **TABLE OF CONTENTS**

### **A. Scientific, Technical, and Management Section**

1	LBR Technical Description .....	1
1.1	Technological Approach .....	1
1.2	Spherical Reflectors .....	3
1.3	LBR Sphere Fabrication .....	4
1.4	Instrument Overview .....	7
1.5	Receiver System .....	9
1.6	Steering/Pointing System .....	11
1.7	Service Gondola .....	12
1.8	Prototype 3 and 5 meter Spheres ... ..	14
1.9	LBR Sensor Package Stratospheric Flight.....	16
2	LBR Demonstration Science.....	17
3	Management .....	19
4	Dissemination of Results... ..	19
5	Future Plans .....	19
6	Project Schedule .....	20

<b>B. References.....</b>	<b>21</b>
---------------------------	-----------

### **C. Biographical Sketches**

### **D. Current and Pending Support**

### **E. Budget and Budget Justification**

### **F. Table of Personnel**

## 1.0 LBR TECHNICAL DESCRIPTION

The Large Balloon Reflector (LBR) development and test program provides a path forward to the realization of 10+ meter telescopes in near-space and serves as a pathfinder for even larger telescope apertures in orbit. In particular, LBR is a progenitor of the TeraHertz Space Telescope (TST) concept to be submitted to the upcoming Astronomy and Astrophysics Decadal Survey. As a demonstration of the scientific potential of an LBR in near space, during the flight tests we will map several star forming regions in the ground state transition of water at 557 GHz and the  $^{13}\text{CO}$   $J=5\rightarrow 4$  line at 551 GHz. The performance of LBR will be validated by performing spectroscopic observations of sources with line strengths determined previously using smaller telescopes and through total power measurements of the Sun, Moon, and planets. The proposed investigation builds upon studies of LBR funded by the NASA Innovative Advanced Concepts (NIAC) program. Both NIAC Phase 1 and 2 studies have been completed (Walker 2014) and key technologies for the flight system validated. A number of LBR subsystems share heritage with the Stratospheric TeraHertz Observatory (STO) which was successfully flown from Antarctica during the 2016-2017 austral summer.

### 1.1 Technological Approach

Water vapor in Earth's atmosphere obscures much of our view of the universe in the far-infrared, creating a major gap in our understanding of the origins of stars, planets, and galaxies (Melnick 1988; Kulesa 2011; Stacey 2011; Walker 2015). It is for this reason that telescopes designed to observe in the far-infrared (*i.e.* terahertz/THz) are placed on high, dry mountain peaks or on the frozen high plateau of Antarctica. However, even these telescopes (*e.g.* ALMA and APEX – Atacama desert, Chile; Heinrich Hertz Telescope – Mt. Graham, Arizona; South Pole Telescope - Antarctica) are essentially blind as a result of atmospheric absorption over much of the far-infrared. The *Herschel* mission placed a 3.5-meter aperture

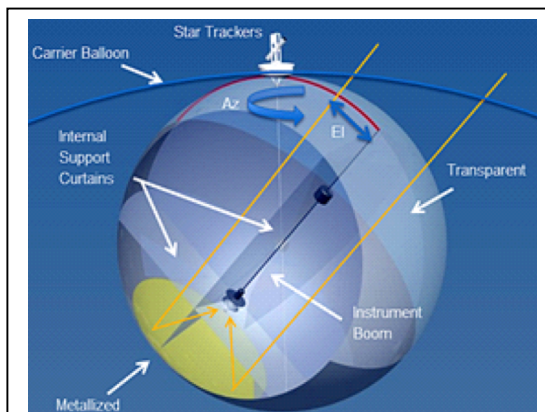


**Figure 2:** LBR Concept. The LBR spherical reflector resides within a transparent carrier balloon, which serves as both a launch vehicle and radome.

into L2 orbit in 2009 and made major advances in THz astronomy and technology.

However,

*Herschel's* 3-year cryogenic mission has ended, leaving behind important new questions to be explored. New capabilities are urgently needed to make forward progress. The James Webb Telescope (JWST) at 6.5 meters will do an excellent job probing the thermal infrared with its dedicated suite of instruments, but it lacks far-infrared coverage and the high spectral resolution needed to disentangle the complex velocity fields associated with

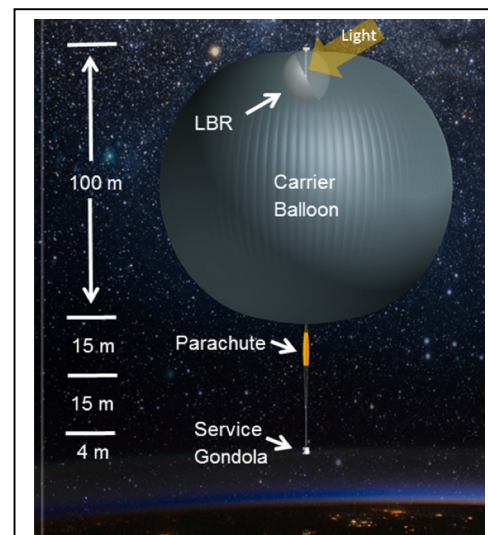


**Figure 1:** LBR Concept. A spherical reflector is formed by the aluminized section of a sphere inflated within the larger carrier balloon.

much of the interstellar medium. The airborne Stratospheric Observatory for Far-Infrared Astronomy (SOFIA) is now available, but for some important astrophysical atoms and molecules (*e.g.* water) is still blinded by Earth's atmosphere. What is required is a large aperture telescope in (near) space capable of conducting far-infrared (THz frequency) high spectral resolution ( $R > 10^5$ ) observations. That is the goal and promise of the Large Balloon Reflector – LBR.

NASA's zero pressure and super pressure balloons (SPB) provide a means of transporting to and maintaining payloads of 2-3 tons in near space. With this capability, it is perhaps possible to construct a 10m carbon-fiber telescope and launch it to near space. However, the combination of stratospheric winds over such a large dish surface and pendulation at the end of a long balloon tether makes pointing the telescope at the required arcsecond levels problematic or impossible.

Instead of attempting to maintain the pointing of a large telescope at the end of a tether, we propose to deploy a telescope in the benign, protected environment *within* the carrier balloon (see Figure 1). The telescope is itself a balloon, spherical in shape, metalized on one hemisphere and anchored to the inner top of the carrier balloon via a rotating azimuth plate (see Figure 2). The carrier balloon serves as both a stable mount and radome for the inner balloon reflector. Light from space first passes through the ~2 mil thick polyethylene skin of the carrier balloon and then through the ~0.5 mil thick Mylar side of the inner balloon. Together these layers have  $\leq 5\%$  absorption at the wavelengths of interest. The incoming light then encounters the aluminized, spherical back surface of the inner balloon and is focused into a receiving system.

3m and 5m prototypes of the LBR concept were created under Phases 1 and 2 of a NASA Innovative Advanced Concepts (NIAC) study, now completed (Walker 2014, Section 1.8). **Now we propose the next logical step: development of a flight system including two 1-day test flights of LBR, the first in September 2019 and the second in September 2020.** These flights will enable the support systems for LBR to be flight-qualified and will allow the end-to-end optomechanical performance to be verified in a true flight environment. A 5m LBR has been chosen as the “sweet spot” aperture.

It is rapidly prototyped; indeed, a 5m early prototype has already been achieved by the team (Section 1.8). Furthermore, most scalable technical challenges for LBR are well-established starting at the 5m diameter. The 5m balloon aperture is large enough to achieve the performance of a ~2.5 meter parabolic reflector, *e.g.* SOFIA. The LBR spherical primary will be used with a spherical corrector. For acceptable aperture efficiency, the inner balloon needs to hold its spherical figure to  $\leq \lambda/8$  of the wavelength of interest. The surface roughness should be  $\leq \lambda/30$ . As an example, the ground state transition of water has a wavelength of 538  $\mu\text{m}$  (557 GHz); at this wavelength the LBR surface roughness needs to be ~18  $\mu\text{m}$  and the spherical figure held to ~67  $\mu\text{m}$ . The required surface roughness is achievable for Mylar under pressure (*e.g.* Clemmons 1964; Cadogan & Scarborough 2001; Elder 1980; Zerbini 1980; Pageos I balloon, ca. 1965 in Figure 3). The spherical figure can be achieved using one or more dielectric support curtains within the



**Figure 3:** Pageos 1 Satellite during tests in 1965: 30.5 m in diameter, 0.5 mil Mylar.

sphere oriented orthogonal to the incident beam. Telescope pointing is accomplished by rotating the azimuth ring and the LBR sphere in elevation. Attached to the rotating azimuth plate on the outside of the sphere and to the instrument module within the sphere are star cameras to determine absolute position on the sky and gyroscopes to maintain pointing knowledge as the telescope slews. The telescope's power system and command and control unit are housed in a conventional gondola service module hanging below the carrier balloon. Low-loss power and fiber optic cables connect the service module to the telescope and instrument. The 'Top Hat' Long Duration Balloon (LDB) experiment launched in 2001 had a similar payload configuration, but with a 1 meter aluminum telescope mounted to the top of a rotating azimuth plate. During the launch (see Figure 4) a tow balloon is used to lift the telescope/rotating plate up while the carrier balloon is being inflated underneath.

## 1.2 Spherical Reflectors

At the heart of LBR is a spherical reflector. Spherical reflectors have a long history in astronomy. This is due in part because a spherical shape is a "natural" result of different types of surface grinding processes. It is also an easy form to measure since all points are at a single distance (the radius of curvature) from the center of the curvature. Due to the isotropic nature of microscopic motion of gases it is also the natural shape for an inflated structure. It has been recognized for several centuries that a spherical reflector is an imperfect focusing element. As shown in Figure 5 a spherical reflector, unlike a parabola, does not bring a plane wave (parallel rays) to a point focus (parallel rays) to a point focus. Radiation from a small section of a



**Figure 4:** Top Hat Balloon Launch in 2001.

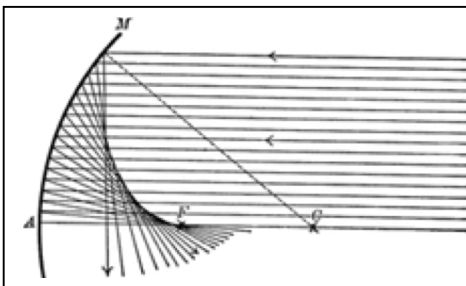


**Figure 5:** Schematic of spherical aberration from a spherical reflector. The rays passing close to the center of curvature (C) are brought to the paraxial focal point (F), while parallel rays incident at greater distances from C cross the C-F axis closer to the reflecting surface.



**Figure 6:** The Arecibo radio telescope. The spherical primary reflector is 1000 ft in diameter. A line feed for 400 MHz operation can be seen hanging below the platform and track. The tip of the line feed is at the paraxial focal point of the spherical primary.

sphere is brought to the paraxial focus (F), located at a distance approximately equal to half the radius of curvature from the surface of a sphere. As more of the sphere is illuminated, the initially parallel rays are focused to a line extending away from the center of curvature (towards A).

The large field of view of a spherical reflector means that to point the beam in different directions, one need only move the feed/receiver in a circular arc centered on the center of curvature of the sphere and having a radius approximately equal to half the radius of curvature of the sphere. The reflector surface, if made larger than the portion utilized at any moment, does not need to move at all. This important advantage was one of the motivations for the design of a 1,000 foot diameter radio telescope; steering such a large structure to point in different directions would be difficult. However, as conceived by Gordon and LaLonde (1961), the Arecibo telescope's spherical primary is held fixed above the surface of a natural bowl-shaped depression. The radius of curvature of the primary reflector of the Arecibo telescope is 870 ft, and the feeds thus move along an arc approximately 435 ft above the spherical surface, as seen in Figure 6. More recently large, spherical reflectors have been constructed for use at optical wavelengths, *e.g.* the 10 meter Hobby-Eberly telescope (Burge et al. 2010).

### 1.3 LBR Sphere Fabrication and Deployment



**Figure 7:** Typical “gore” pattern sections used in most scientific balloons.

LBR uses the natural shape of an inflated balloon to create a spherical reflector. Three different approaches to fabricating LBR were investigated in our NIAC study. The first approach uses the typical gore or “banana peel” technique (Figure 7) employed in the fabrication of large scientific balloons. This makes use of flat sheets of film cut into a pattern and then sealed together to create a 3-dimensional structure. For a small number of gores under low pressure the volume looks faceted. Higher pressures are required to stretch or deform the material into the more spherical shape. It will also create a line of higher stress in the centerline of the gore due to having to distort a 2D flat panel into a 3D shape. Thus, if too few gores are used, it will exceed the structural limits of the material and fail, often catastrophically. This can be remedied by increasing the number of gores, but this

further creates an undesirable stiffening of the structure at the apex and nadir of the sphere due to converging seam tapes. The structure thus has a variable stiffness along its length which has to be accounted for in the structural analysis such that the final shape will be the desired sphere. Whereas this is usually fine for large scientific balloons using large deformation polyethylene, it presents more difficulty for the stiffer materials and smaller volumes associated with LBR. Another problem is the seaming together of longitudinal bands of flat material. Some of the structural elements, such as the seam, do not scale well at the smaller sizes.

An alternate construction method is similar to that employed in fabricating soccer balls (and geodesic domes), where hexagonal and pentagonal sections are seamed together into a Goldberg polyhedron (see Figure 8). This approach provides more uniform loading over the gore approach and does not suffer from a high concentration of seams near the sphere poles. The polyhedron can be constructed from an icosahedron with the 12 vertices truncated such that one third of each edge is cut off at each of both ends. This can be further improved by “casting” the polymer on a 3D mandrel, in which case the element takes on the requisite 3D shape, thus eliminating stress risers.

The structure of the LBR sphere is shown in FO1. The structure is made of two hemispherical hull sections, one that is transparent and one that is metalized to be reflective to the THz signal. One or more internal orthogonal curtains provide shape stability and serve as mounts for the optical

signal corrector and signal receiver. The whole structure is folded and packaged in a container for installation inside the carrier balloon on the flight line. The packed LBR remains in this protective container during launch. At approximately 65,000 ft. the balloon has expanded to where LBR can be extracted from its protective container. The inflation of the sphere is initiated using the He from within the carrier balloon as the fill gas. This offers the advantage of being able to use the higher relative density He gas at altitude. The sphere is only partially filled and is metered such that the sphere continues to expand as it ascends. It becomes fully inflated when it reaches float altitude. Two blower assemblies maintain the selected differential pressure to provide the optimum shape and stability. The LBR hull and internal curtains are made of very thin film that have been selected to be >98% transparent to the target signal. FO2 illustrates the flight profile for a 1 day LBR test flight using a standard zero pressure balloon as the carrier balloon. Flights of 100+ days will be possible using NASA’s Super Pressure Balloon (SPB).



**Figure 8.** Prototype “soccer ball” sphere constructed at Nexolve Inc. Individual hexagonal panels can be formed to high precision on a mandrel and then thermally bonded together to create a sphere. This approach has the advantage of providing more uniform loading and a reduced number of seams at the poles compared to a sphere constructed from gores.

### 1.1 Instrument Overview

A block diagram of the Instrument Unit (IU) is shown in Figure 9. LBR’s optics are designed to provide a 4x4, 53" full-width-half-maximum (FWHM) diffraction limited beams at the frequency of the astrophysically important ground state water line (557 GHz). The IU includes a

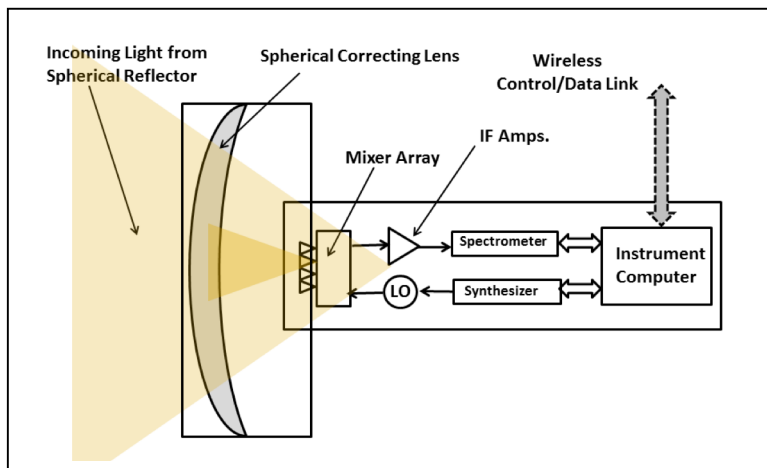


**Figure 9:** LBR’s Instrument Unit (IU). THz light from the 2.5 meter reflector enters the optical system which corrects for spherical aberration and focuses it into a low-noise THz receiver system. The receiver produces a power spectrum of the THz light which is passed on to the instrument computer and wirelessly to the telecommunications system.

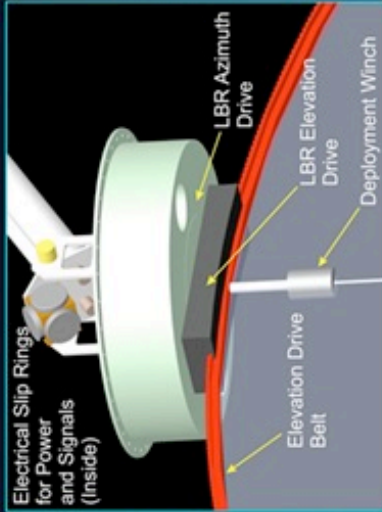
refractive spherical corrector and 16 pixel Schottky receiver system. It is rigidly mounted inside the sphere at the intersection of three orthogonal support curtains at the focus point of the spherical reflection surface. The IU mount provides tip-tilt for fine motion control. Focusing is achieved by moving the whole assembly axially. During flight the LBR beam quality will be routinely measured and optimized on a calibration sources (e.g. the Sun, Moon, and planets).

# THz Sub-Orbital Large Balloon Reflector (LBR)

F01

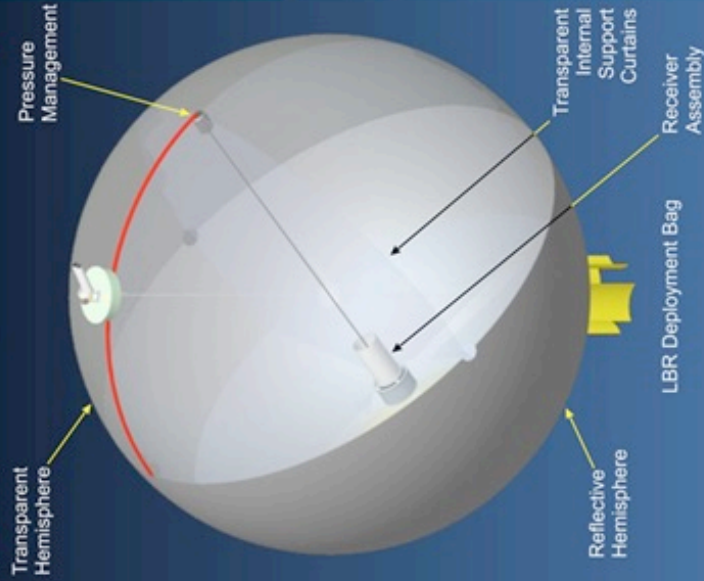
## Top Plate Assembly

Mounts to the Carrier Balloon Top Ring



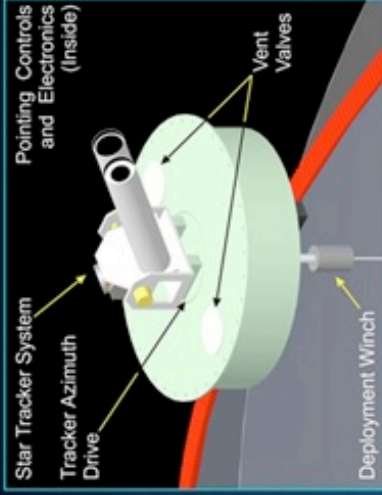
## Spherical Reflector Assembly

20 Meter Diameter  
Pressurized to 1 mbar with Helium  
Azimuth Range : Unlimited  
Elevation Range: 0° to 60°



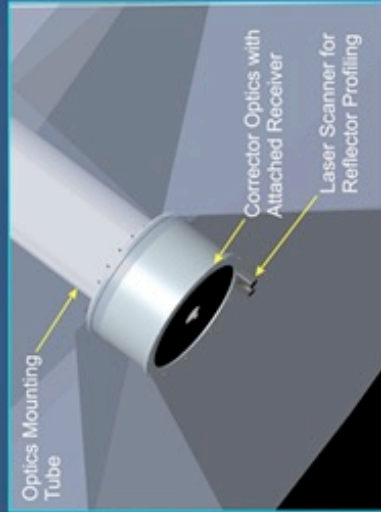
## Top Plate Assembly

Diameter: 2m Depth: 0.75m



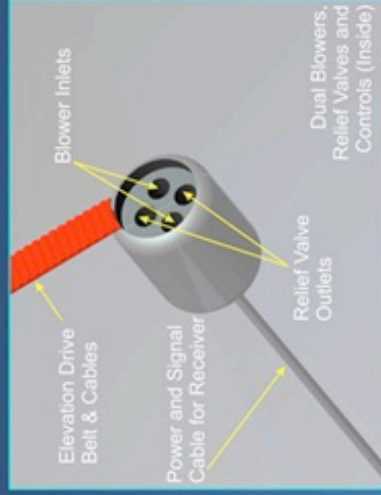
## Corrector and Receiver Assembly

Adaptive Optics Axial Focus Control



## Pressure Management

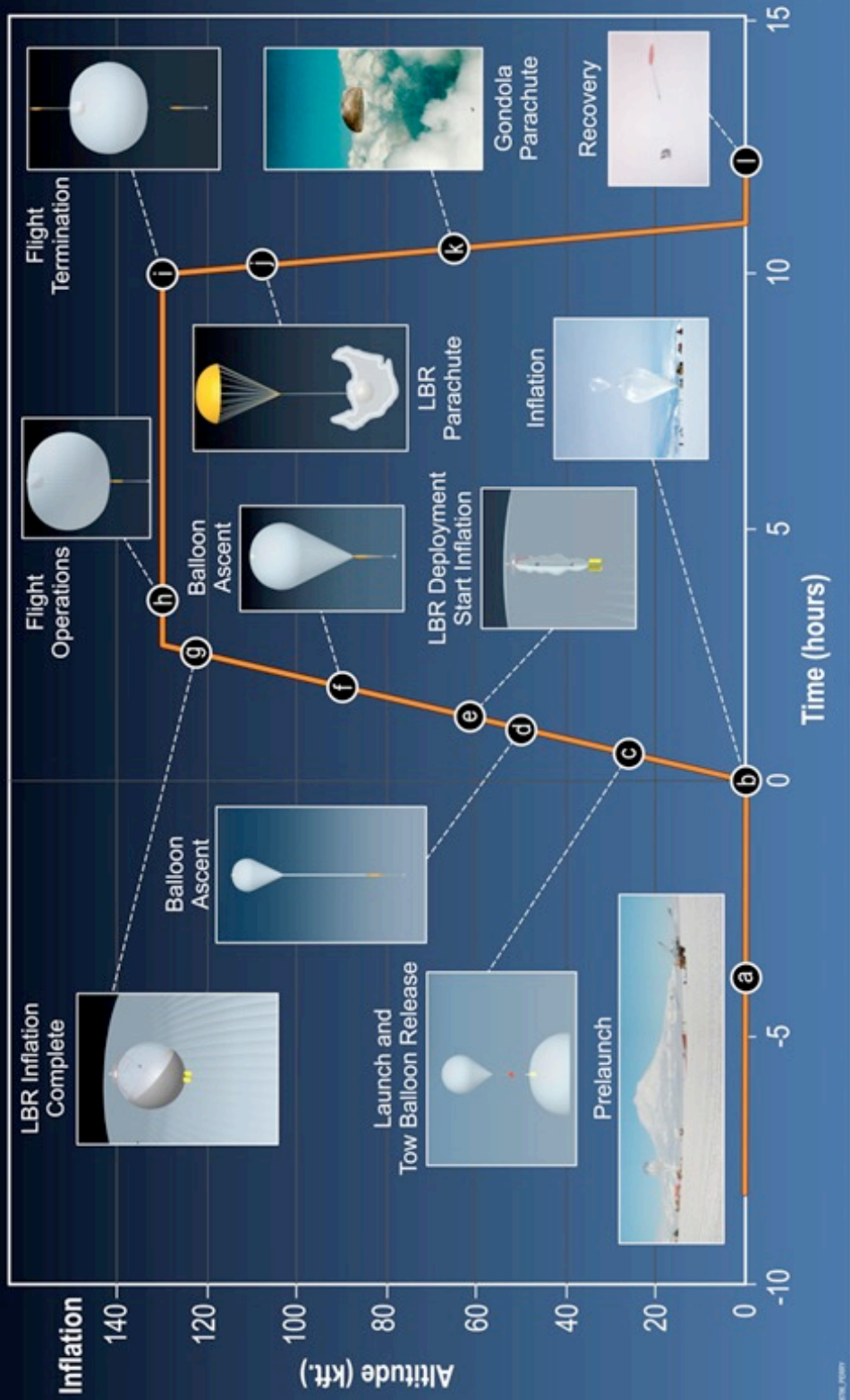
Constant Differential Pressure  
Redundant Blowers and Relieve Valves





# Typical LBR Balloon Flight Profile

F02



A detailed design of the IU required for use with the 5 meter LBR was performed under NIAC and a prototype constructed. A photograph of the completed unit is shown in Figure 10. The prototype IU was tested in the laboratory and found to meet functional requirements. In the NIAC version an offset Gregorian corrector similar to that being used on Arecibo was employed. For the first test flight we will instead use a simple refractive corrector designed using geometrical optics tools and optimized using the more sophisticated modelling software GRASP (General Reflector Antenna Software Package). A prototype of the refractive corrector was successfully tested at ~100 GHz using a 30 cm spherical reflector (see Figure 11). The lens together with the array (see Figure 12) will be measured using a submillimeter wave near-field scanner to evaluate the aperture phase correction of the lens and horn illumination.

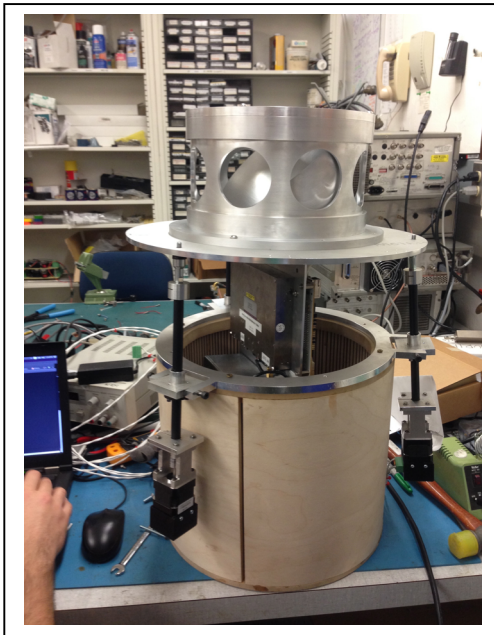


**Figure 10.** Instrument Unit (IU) developed in NIAC Phase II. In this orientation light from the spherical reflector enters the IU from above where it encounters a spherical corrector consisting of two mirrors. The corrector collapses the focal line produced by the spherical reflector to a focal point just within the aperture of a waveguide feedhorn.

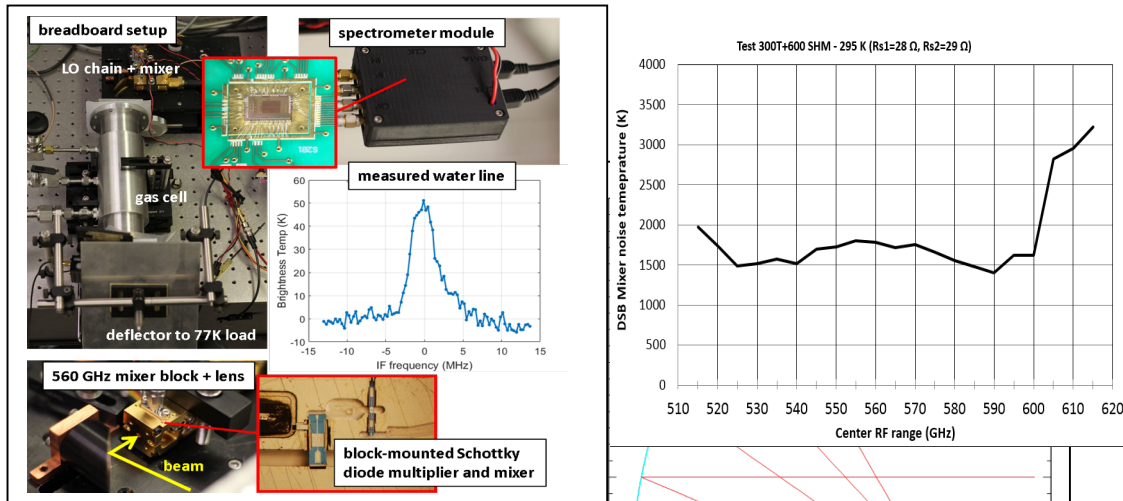


**Fig. 12:** LBR Test Receiver: (a) Clockwise from bottom: A 560 GHz Schottky diode mixer mounted in a waveguide block; a breadboard prototype receiver with a gas cell of water vapor in front of a cold load; a CMOS spectrometer chip mounted in a compact module; and a measured water-line spectrum demonstrating LBR’s receiver architecture in an end-to-end prototype. (b) Typical JPL 560 GHz subharmonic mixer noise temperature. 1000 K DSB is expected for LBR when fabricating these devices with an optimized epi structure for mixers

**Figure 11.** LBR Spherical Corrector. *Right:* Prototype refractive spherical corrector illuminating a 30 cm spherical reflector. *Left:* Ray tracing diagram showing of system.

## 1.2 Receiver System

Adequate mapping of the  $^{13}\text{CO}$  5-4 and  $\text{H}_2\text{O}$  ground state lines at 551 and 557 GHz with ambient temperature receivers on 1 day test flight **requires the multi-beam advantage of heterodyne receiver arrays**. To achieve adequate SNR, particularly in the 557 GHz water line, total integration times ranging from 5 to 60 minutes per beam will be required. To achieve sufficient sampling for small 5-10’ maps, an array receiver with at least 10 pixels is required. Furthermore, a focal plane array eases initial pointing assessments and allows continuous monitoring of the full focal plane. The proposed 16-pixel 557 GHz receiver system is based on a Schottky diode mixer architecture recently demonstrated at JPL. The receiver consists of 90-95 GHz CMOS-based W-band synthesizer, which is then amplified and frequency multiplied (x3) to pump a subharmonic 557 GHz mixer. The JPL-fabricated multiplier and mixer chips are proven designs.

The LBR 557 GHz receiver approach has been demonstrated end-to-end as shown in Fig. 12. For these tests the IF signal at 1.5 GHz was amplified, filtered, and sampled over a folded Nyquist bandwidth using the identical JPL/UCLA-designed CMOS spectrometer to be flown in LBR. In the 25 cm long gas cell, room-temperature water vapor is introduced at 8 mTorr, with a background temperature through the cell's window of 77 K from a load submerged in liquid nitrogen. Fig. 12 shows the measured baseline-normalized (through LO frequency-switching) water spectrum over a 30 MHz bandwidth and 300 kHz bin resolution, and the noise level of 2.4 K is consistent with the integration time of 120 s, the mixer noise temperature, additional losses from the atmospheric optical path, imperfect IF filtering, and digital FFT-based spectral estimation. These results demonstrate the high maturity of the components, circuit architecture, and measurement process that LBR will use, showing how LBR's critical Schottky diode mixer/multipliers and digital spectrometer can be readily interfaced together for successful, low-noise acquisition of water's 557 GHz emission spectrum.

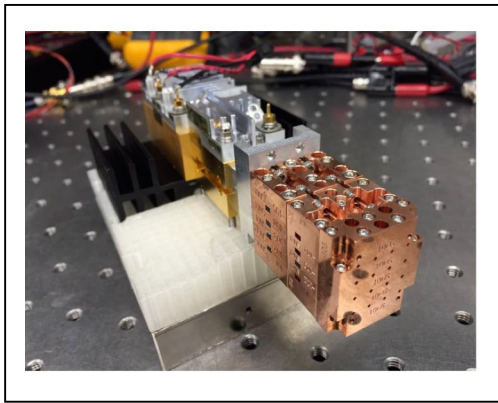


**Fig 13.** Photo of a prototype 16-pixel 1.9 THz local oscillator chain (4x4 configuration). The LBR 16-pixel 557 GHz receiver will use this mechanical architecture.

The technical approach for the 16-pixel focal plane array receiver will also leverage a 3D packaging capability recently demonstrated at JPL, funded through NASA's Strategic Astrophysics Technologies program (SAT) to enable multi-pixel local oscillator sources. The receiver front-end will be very similar to the module shown in Fig. 13, which includes a 16-pixel LO at 1.9 THz recently developed at JPL. The JPL provided 16-pixel 557 GHz receiver system will use a single low-power CMOS synthesizer (developed through a previous NASA MatISSE program), and 16 signal paths (stacked in a 4x4 array scheme) each of them featuring a COTS GaAs amplifier, a JPL broad-band 280 GHz tripler and a JPL 557 GHz Schottky diode based subharmonic mixer.

For the first flight, a simplified version of the 16-pixel array receiver will be flown, consisting of the same architecture but with only 4-pixel signal paths populated in the mechanical blocks. The packaging will be similar. The 16-pixel IF amplifier modules will be provided by Arizona State University based on SiGe Low Noise Amplifiers followed by a cascade of power amplifiers to achieve the output power required by the back-end spectrometers. The specifications of the IF modules are:

- <50K noise temperature
- 500MHz-3 GHz frequency range
- >90dB gain
- <62.5 mW power consumption per channel
- >+10 dBm 1dB compression point

The CMOS spectrometer was developed by UCLA with collaboration from JPL and validated in a 2013 MatISSE effort. The spectrometer is implemented in 65 nm CMOS technology (the same technology as the Apple iPhone 4s) and combines a 7-bit sub-ranging and 4 way interleaved ADC with a 4-parallel Cooley-Tukey radix-2 FFT processor and 56 bit data accumulator. Table 1 summarizes key instrument parameters.

**Table 1: LBR Receiver System Specifications**

SPECIFICATION	556 GHz Receiver (Flight 1)	556 GHz Receiver (Flight 2)
Center Frequency	555 GHz	555 GHz
RF Tuning Bandwidth	550-560 GHz	550-560 GHz
Number of Pixels	4 Pixels (2x2 integrated)	16 Pixels (4x4 integrated)
Horn Type	Diagonal	Diagonal
Pixel Spacing	~ 5.4 mm (horn-to-horn)	~5.4 mm (horn-to-horn)
Receiver Noise Temperature (DSB)	< 3000 K (~2000 K expected)	< 3000 K (~2000 K expected)
Temperature of Operation*	0C to 50C (25C nom.)	C to 50C (25C nom.)
Pressure	3-1013 mbar	3-1013 mbar
Relative Humidity	<90% (non-condensing)	<90% (non-condensing)
Power Dissipation/Margin	12 W typ. (+50% margin)	40 W typ. (+50% margin)
Mass/Margin	7 Kg (+30% margin)	10 Kg (+30% margin)
Individual Power Control	Yes (>5 dB tuning)	Yes (>5 dB tuning)
Technology	Solid State Schottky Frequency Multipliers/Mixers	Solid State Schottky Frequency Multipliers/Mixers
IF Frequency	1.5 GHz	1.5 GHz
IF Noise Temperature	<50K	<50K
Spectrometer Technology	CMOS	CMOS
Spectrometer Bandwidth	500 MHz / 512 channels	500 MHz / 512 channels
Spectral Resolution	< 1 MHz	< 1MHz
Document Deliverables	<b>Operations</b> document, including multiplier biases for operation and do not exceed values. Tuning sheet <b>test data</b> , incl. performance vs: 1) operating temp, 2) frequency, 3) multiplier bias.	

### 1.3 Steering/Pointing Mechanisms

As described earlier, coarse pointing of LBR is achieved by rotating the whole spherical reflector in elevation and azimuth (see F01). The azimuth rotation range is unlimited. The elevation range will be  $-10^{\circ}$  to  $70^{\circ}$ . Wireless communication is used for data transmission and instrument control. A slip ring assembly is used to provide electrical power to LBR. The azimuth rotator is powered by a direct drive servo motor with a high-resolution encoder, while the elevation change will be accomplished by driving a toothed belt that is secured to the circumference of LBR sphere. This belt is driven by a servomotor powered anti-backlash gear arrangement. A linear high resolution encoder provides accurate elevation positioning. These drive systems are housed in the bottom of the carrier balloon's top plate assembly along with the azimuth/elevation drive for the star camera telescope that is mounted on the top plate assembly. Fine pointing is achieved by tip-tilts of the instrument module.

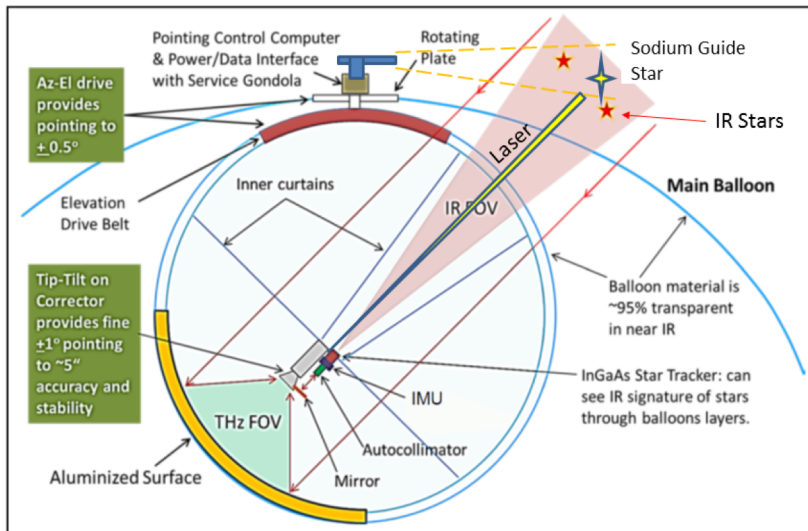


**Figure 14.** LBR Pointing Systems. The performance of both an infrared star camera and sodium guide star system will be evaluated in their ability to obtain pointing knowledge.

Two types of star cameras will be evaluated in their ability to determine the pointing of LBR relative to the background stars. The first is a  $\sim 1 \mu\text{m}$  wavelength infrared camera mounted on the back of the instrument module, facing the incoming light (see Figures 9 & 14). Lab measurements indicate the balloon material is  $\sim 90\%$  transmissive at this wavelength making it possible to observe many IR stars directly through it. However, there is a

possibility that wrinkling or seams in the gore material of the outer balloon may interfere with imaging along some lines of sight. For this reason, there will also be a  $589 \text{ nm}$ ,  $\sim 1 \text{ watt}$  laser beam projected from the front of the instrument module to generate a sodium guide star in the mesospheric sodium layer located  $\sim 50 \text{ km}$  above the balloon (Figure 14). Due to its weight the laser itself will be mounted on the gondola and the beam conveyed to the instrument module via a low-loss optical fiber. A camera located on a pivot mount on the balloon apex will image the sodium guide star against the background stars to provide the pointing knowledge required to close the servo loop. Using a modest sized Fresnel lens and bandpass filter both laboratory and day time measurements indicate the sodium guide star can be readily detected both day and night (Hart, Jefferies, and Murphy 2016). With a similar servo loop on the STO gondola pointing accuracies of better than  $5''$  were achieved. This performance meets our pointing goal of  $\sim 15''$ , corresponding to  $\sim 1/4^{\text{th}}$  our diffraction limited beam at our target observing frequency,  $557 \text{ GHz}$ .

#### 1.4 Service Gondola

A Service Gondola suspended underneath the carrier balloon (see Figure 15) will carry and protect the command and control computer, the power system, and the balloon control and telecommunication systems, which are needed to support the LBR instrument and mission. The design is based on the heritage of several gondolas built and flown by APL. The gondola and all its subsystems will be designed, built, and tested by APL, with the exception of the balloon control and telecommunications package which is provided by CSBF. The service gondola can be divided into four main components: the structure, the power system, the command and data handling system, and the telecommunication system. Table 2 and 3 provide current best estimates for

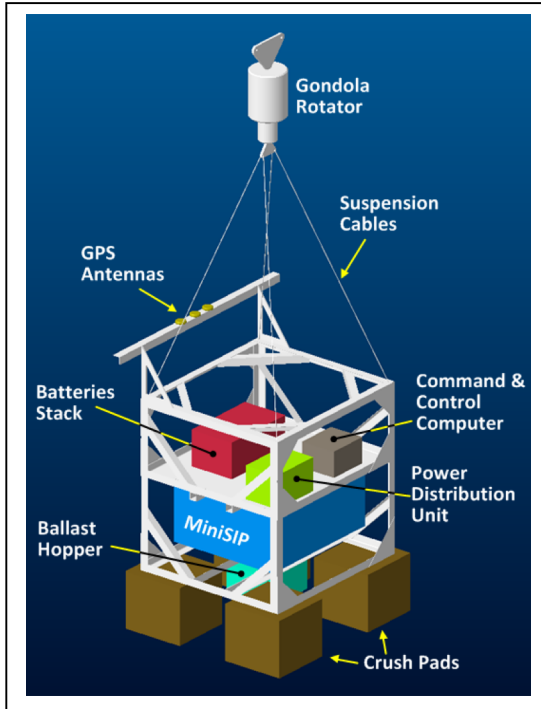
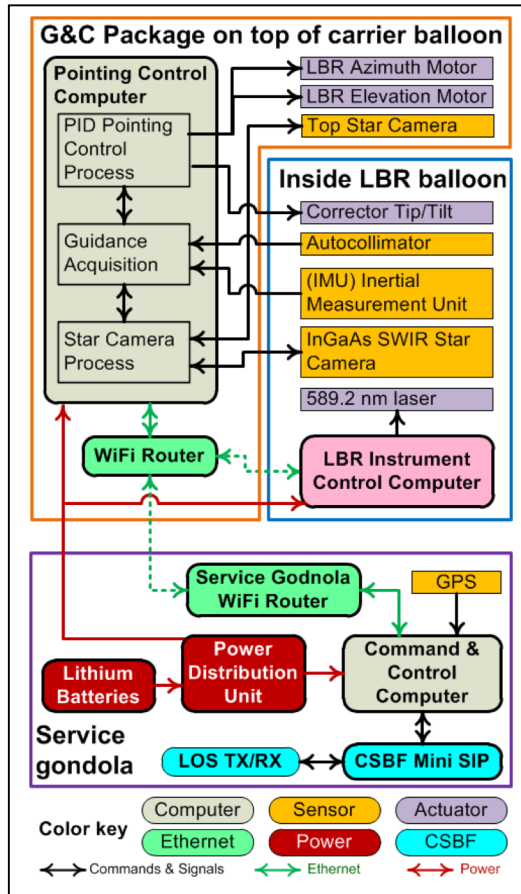


**Figure 15.** Conceptual design of the LBR Service Gondola.

mass and power of LBR.



the

<b>Table 2: Estimated LBR System Mass Summary</b>		
	Mass	
	lbs	kg
<b>Service Gondola</b>		
<i>Frame</i>	536	244
<i>Avionics</i>	25	11.4
<i>Sodium Laser</i>	66	30
<i>LBR Power</i>	525	238
<i>Harness</i>	20	9
CSBF provided equipment:		
<i>Rotator</i>	150	68
<i>SIP</i>	350	159
<i>SIP Power</i>	100	45
<i>Antennas</i>	46	22
<i>Ballast Hopper</i>	23	10
<i>Crush Pads</i>	80	36
<b>Total Service Gondola (without ballast)</b>	<b>1921</b>	<b>873</b>
<b>Flight Train (CSBF provided equipment)</b>		
<i>Parachute Assembly</i>	543	246
<i>Standard Flight Train Components</i>	215	98
<b>Total Flight Train</b>	<b>758</b>	<b>344</b>
<b>LBR Spherical Telescope</b>		
<i>Sphere Structure</i>	40	18.2
<i>LBR Elevation Drive Assembly</i>	10	4.5
<i>LBR Azimuth Drive Assembly</i>	10	4.5
<i>Balloon Top Plate Assembly</i>	61	28
<i>LBR Harness</i>	10	4.5
<i>LBR Deployment System</i>	10	4.5
<i>LBR Sphere Pressurization Assembly</i>	5	2.2
<i>Instrument Module</i>	31	14
<b>Total LBR Spherical Telescope</b>	<b>177</b>	<b>80.4</b>
<b>GNC Package on Top of Balloon</b>		
<i>IMU</i>	2	1
<i>Star Cameras</i>	5	2.3
<i>Mount and Elevation System</i>	10	4.5
<i>Harness</i>	2	1
<b>Total GNC Package</b>	<b>19</b>	<b>8.8</b>
<b>Total Carried Mass (without ballast nor balloon)</b>	<b>2875</b>	<b>1307</b>
<b>Launch Stabilizer (Ethafoam Ring on top of Balloon)</b>	<b>40</b>	<b>18</b>
<b>Balloon, Raven W29.47-2x-P (LDB: Zero Pressure)</b>	<b>3675</b>	<b>1667</b>
<b>Total Mass Including Balloon (without ballast)</b>	<b>6590</b>	<b>2992</b>

<b>Table 3: Summary Estimated LBR System Power</b>		
	Average	Peak
	[w]	[w]
<b>Instrument</b>		
<i>Receiver Module</i>	40	60
<i>IR Camera</i>	20	30
<i>Sodium StarLaser</i>	20	100
<b>Total Instrument</b>	<b>80</b>	<b>190</b>
<b>Gondola and G&amp;C</b>		



	<i>Pointing</i>	30	150
	<i>Avionics</i>	50	80
<b>Total Gondola and G&amp;C</b>		<b>80</b>	<b>230</b>
LBR			
	<i>Pointing</i>	50	150
	<i>Pressurization System (2 each)</i>	20	200
<b>Total LBR</b>		<b>70</b>	<b>350</b>
<b>Total Power</b>		<b>230</b>	<b>770</b>

The approach for the power and data link between the service gondola and the LBR system and GNC package on top of the carrier balloon is shown in Figure 16. Power and telecommunication links will be accomplished using two separate approaches. For communications we baseline Ethernet WiFi, with a WiFi router on the service gondola communicating to another router on top of the balloon. The top WiFi router performs networking connections between the WiFi on the service gondola, the Pointing Control System (PCS) computer to which it will be connected via hard Ethernet wire, and the Instrument Control Computer inside the LBR balloon which also has WiFi capability. This obviates the need to send data signals from the LBR instrument control computer to the service gondola C&C computer via an extremely long (up to 1000 feet) Ethernet cable, two slip-ring assemblies and a set of bulkhead connectors, which could likely cause signal degradation.

For power distribution we will utilize a long power cable equal in length to that of the fiber used to convey the guide star laser beam. The cable and fiber run from the top of the service gondola through the rotator assembly (via slip-rings), along the furled parachute and the sides of the carrier balloon, to reach the LBR on top (see Figure 16). They will be stitched along the carrier balloon support guy lines at opposite sides of the balloon. This balances the mass of the wires and prevents the balloon from listing to one side causing the top assembly and the LBR to be off center. The challenge for the power lines is how to minimize the power wires mass and voltage loss along the cables since the cable length will be on the order of 850 to 900 feet. However, the TopHat balloon mission was able to accomplish this. The projected loss in laser power along the fiber run is projected to be only ~15%. To prevent imbalance the power and fiber cables will be equal mass and run along opposite sides of the carrier balloon.

### 1.8 Prototypes: 3 meters and 5 meters

Figure 17 (left) is a photograph of the 3 meter diameter, rooftop LBR prototype developed in Phase I of the NIAC LBR investigation. The prototype was constructed to gain experience with the technological approaches needed to realize and operate a full size LBR. The prototype had all the key elements of the flight version. The sphere was purchased from a toy company and is formed from 0.8 mm thick, thermoplastic polyurethane (TPU) gores. For the LBR flight model a higher quality “soccer ball” sphere made from thin Mylar film will be used. The gores of the 3 meter prototype are thermally bonded together to create a spherical shape. The plastic sphere had a 1 meter long zipper through which hardware (and people!) enter and leave. As will be the case for the flight model, a blower is used to inflate the balloon with outside air. For the flight version the ‘outside’ air is the helium gas that fills the carrier balloon. The pressure in the balloon is regulated to be just above ambient. For the 3 meter prototype a reflective surface was first created by

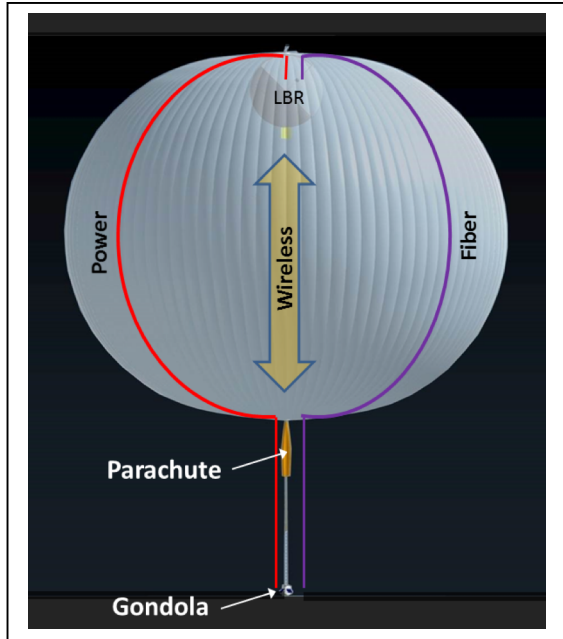


**Figure 16.** Sphere Interconnectivity.

spraying a 1 meter diameter section of the sphere with metallized spray paint, though later we found that aluminized Mylar sheets stretched over the outer surface could achieve the same high reflectivity. The optical performance of the rooftop LBR was characterized by performing a series of scans across the position of a test transmitter and the Sun, yielding diffraction limited performance (Figure 17, inset). A number of valuable lessons were learned in the construction and operation of the LBR rooftop prototype. In Phase II of the NIAC a 5 meter version (same size as being proposed here) of the LBR sphere was constructed in a high bay at the Southwest Research Institute (see Figure 17 left). The sphere included the dielectric support curtains and was filled with a mixture of helium and nitrogen gas to achieve neutral buoyancy. The structure achieved a spherical shape to better than 1%, meeting both the surface and figure tolerance requirements. For this experiment an inexpensive latex sphere was used.

For the flight version a much more robust Mylar sphere will be employed. The 5 meter sphere included all the key elements (elevation drive, azimuth drive, inflation and pressure control blowers, metallized reflector, etc.) that will be required for our LBR system.

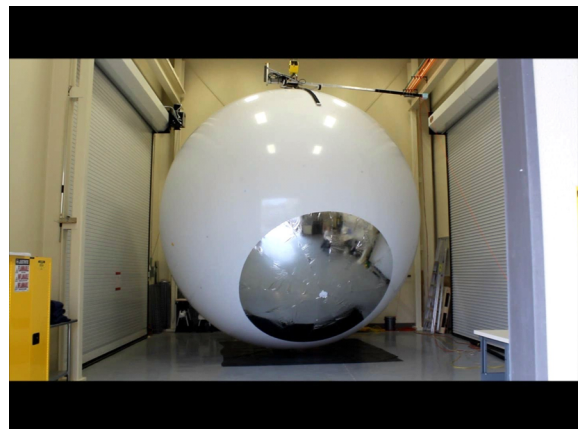
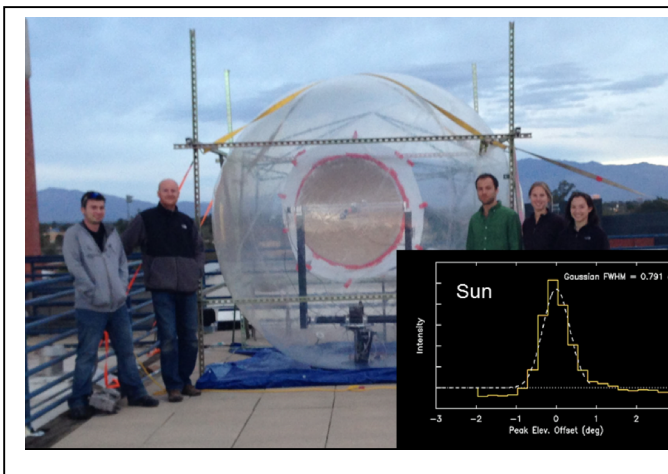
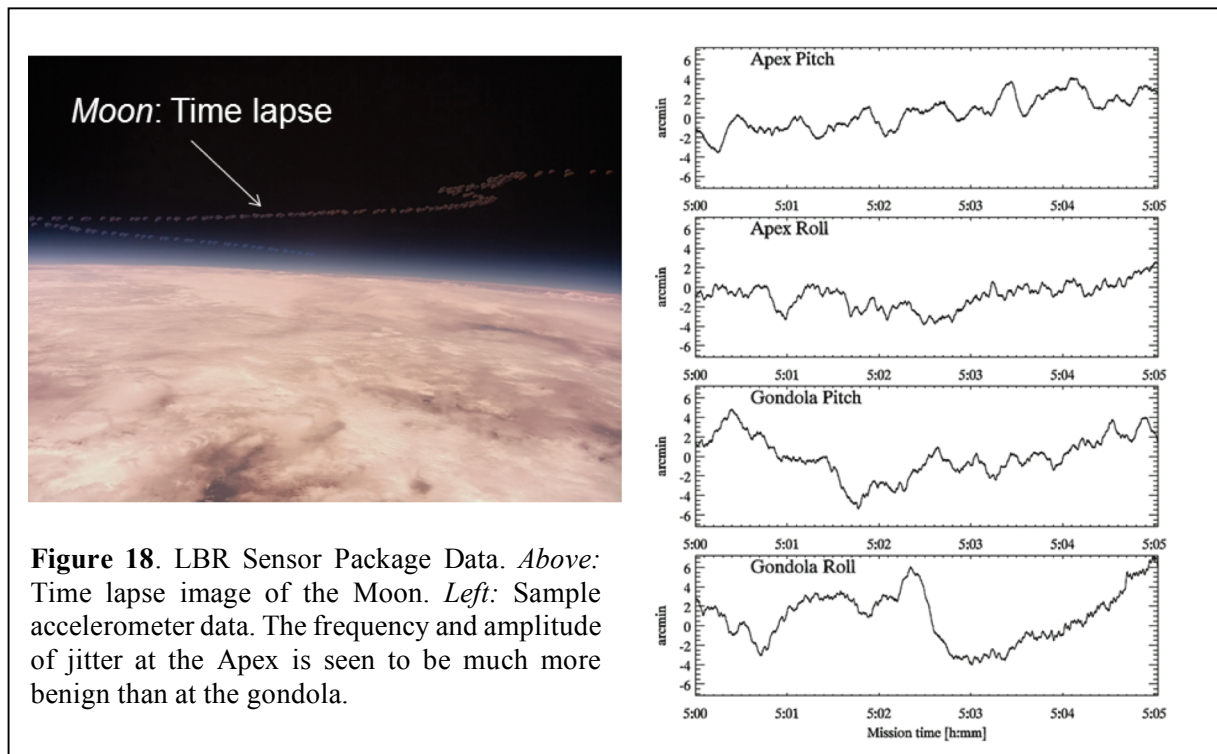


**Figure 17: Left: 3 meter LBR rooftop prototype.** The rooftop prototype is a fully functional 3/5<sup>th</sup> scale model of the flight version of LBR designed to operate at 115 GHz. A Sun scan made with the prototype (bottom right) yielded diffraction limited performance. **Right: Steerable, full scale 5 meter LBR prototype sphere.** The sphere includes dielectric sheets to ensure a spherical shape and provide a stable mounting point for the instrument module. Optical metrology of the 5 meter indicated it maintained its spherical shape to better than 1%.

## 1.9 LBR Sensor Package Stratospheric Flight



The Mid-Term Review for the LBR Phase II NIAC effort was held in Washington, DC on April 27<sup>th</sup>, 2015. The panel consisted of far-infrared astronomers, instrumentalists, and ballooning experts. The consensus was that, based on the work presented, LBR could indeed be built and flown as a stratospheric balloon payload. The review panel concluded that what would ultimately limit the size of LBR is the ability to point it. Intuition suggests that, owing to a closer proximity to the center of mass and the dispersive effects of the balloon on wind gusts, having LBR attached to the inside top-center of the balloon would be more stable than having it suspended from the gondola. However, this needed to be proven. The suggestion was made to fly an accelerometer/camera sensor package both on the top of a balloon and on a gondola underneath to obtain the required empirical data. This idea was presented to NASA and a “piggy-back” stratospheric flight was approved for summer 2015. The sensor packages for the flight were designed and built by our team and launched from Ft. Sumner, NM on Sept. 4<sup>th</sup>, 2015. The flight lasted for several hours during which time data was obtained from both sensor packages. A time lapse image of the Moon and sample accelerometer data taken during the flight are shown in Figure 18. A Fourier analysis of the data shows there are several oscillation modes on top of the balloon, but all with periods greater than 5 seconds which can be readily dealt with by the LBR pointing system. However, the observed oscillations on the gondola had both greater amplitudes and shorter periods (between 2 and 0.8 sec). Thus, for improved pointing control, it is preferable to have the LBR attached internally to the top-center of the balloon than suspended from a gondola.

## 2. LBR Demonstration Science

With less than 1% of the Earth’s atmosphere left between it and the hard vacuum of space, a stratospheric LBR can observe any number of THz atomic and molecular transitions, as well as the thermal emission associated with astrophysical sources. A plot comparing the atmospheric

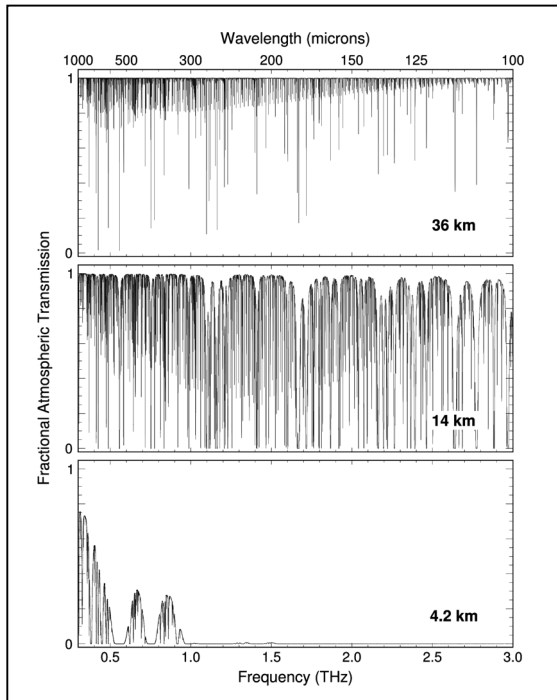


**Figure 20.** THz atmospheric transmission for typical weather conditions from mountain-top site (4.2 km) airborne altitudes (14 km), and balloon-borne altitudes (32 km). (from Walker 2015; see also Melnick 1988)

Fortunately, at altitudes accessible to balloon-borne telescopes the telluric water absorption lines narrow sufficiently to allow Doppler shifted observations of water. Figure 22 is a zoom-in on the  $1_{10} - 1_{01}$  atmospheric line of ortho-water from an altitude of  $\sim 130,000$  ft. At velocity offsets  $>30$  km/s atmospheric transmission is  $>50\%$ , permitting observations toward a wide variety of planetary, galactic, and extragalactic objects. The velocity of an object relative to the Earth varies with the time of year. Table 4 lists the minimum and maximum Doppler shifts for a small subset of sources, all of which can be observed during the course of the year in the northern hemisphere with LBR. Assuming a mid-September launch from Ft. Sumner, NM suitable target sources for LBR include W3, W51, NGC 7538, and Sgr B2. All these objects were detected in the 557 GHz transition of  $\text{H}_2\text{O}$  and the 551 GHz transition of  $^{13}\text{CO}$  by *SWAS* using a heterodyne instrument similar to that baselined for LBR, making them excellent test sources. The *SWAS* observations of water (e.g. Figure 22) often show complex line profiles that are extended relative to the  $3.3' \times 4.5'$  *SWAS* beam. Such line profiles are expected to vary significantly with beam size (Walker 2015, Ch. 2). With its  $\sim 2.5$  meter effective aperture and  $4 \times 4$  array receiver, LBR will sample a  $5' \times 5'$  region of the sky with  $1'$  angular resolution with each

transmission at balloon, airborne, and high mountain top sites is provided in Figure 20 (Walker 2015, Melnick 1988). **A crucial and unique application for a balloon-borne THz telescope is the observation of Galactic and extragalactic water, which cannot be observed either from the ground or from SOFIA.** Water plays a central role in star formation and the evolution of our Solar System, and following its chemistry and dynamics from molecular clouds to hot cores to debris disks is of critical importance to star and planet formation. Besides being seen toward molecular clouds, water vapor emission has also been observed in the envelopes of evolved stars (Neufeld et al., 2011), emanating from comets (Neufeld et al., 2000) and, more recently, asteroids (Küppers et al., 2014).

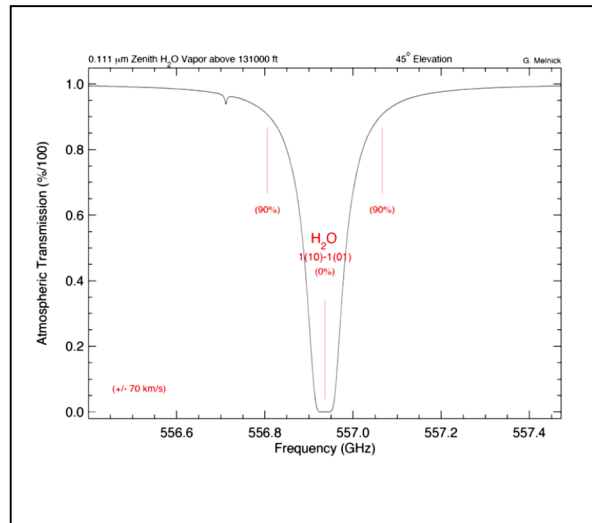


**Figure 21:** Atmospheric transmission of the 557 GHz  $\text{H}_2\text{O}$  line at  $45^\circ$  zenith distance from  $\sim 130,000$  ft. For Doppler shifts of  $>30$  km/s atmospheric transmission of  $>50\%$  are obtained. (Assumed 1976 U.S. Standard Atmosphere yielding a pressure at 40 km of 2.8 mbar)

integration. A comparison of line profiles between *SWAS*, LBR, and *Herschel* will aid in untangling the dynamics and physical conditions within the underlying objects.

Observations from *SWAS* (Figure 22) suggest a  $T_{rms}$  of  $\sim 0.1$  K should be sufficient to robustly detect both the 557 GHz transition of water and the 551 GHz transition of  $^{13}\text{CO}$  toward our target sources. Assuming a conservative single sideband receiver noise temperature of  $\sim 4000$  K, an atmospheric transmission of 50%, and a spectrometer resolution of  $\sim 0.5$  km/s, LBR should reach

this noise level in all 16 pixels within  $\sim 2$  hours. Both absolute position switching and frequency switching will be employed during the test flights. The exceptional stability of Schottky receivers, together with the wide bandwidth of the CMOS spectrometers, make frequency switching an attractive option for achieving maximum observing efficiency.

In addition to spectroscopic observation of known sources, the quasi-optical performance of LBR will be assessed by making beam maps and scans of strong continuum sources, *e.g.* the Sun, Moon, and planets (see Walker 2015, Ch. 8).

Source	J2000 Coordinates		Min. Velocity (km s <sup>-1</sup> )	Max. Velocity (km s <sup>-1</sup> )	LSR Velocity (km s <sup>-1</sup> )
	RA (h m s)	Dec (° ' ")			
M17SW	18 20 22.1	-16 12 37.0	-23.7	36.0	20.0
Mon R2	6 7 40.2	-6 23 28.0	-2.8	49.6	5.0
NGC 1333	3 28 57.8	31 21 2.0	-14.6	44.3	8.0
NGC 1333 IRAS4A	3 29 10.5	31 13 31.0	-14.6	44.3	8.0
NGC 2024	5 41 44.5	-1 55 35.0	1.4	56.0	11.0
NGC 2071	5 47 5.0	0 21 48.0	-1.4	54.1	9.0
NGC 7538	23 13 45.4	61 28 10.0	-83.3	-51.1	-57.0
OMC-1	5 35 14.5	-5 22 37.0	0.7	53.7	9.0
Rho Oph A	16 26 23.4	-24 23 2.0	-36.7	23.5	4.0
S140	21 43 1.7	66 3 23.0	-31.1	-8.9	-7.1
Sgr B2	17 47 19.7	-28 23 7.0	19.4	79.4	60.0
W3(OH)	2 27 4.1	61 52 22.0	-71.6	-28.5	-46.4
W49	19 10 13.5	9 6 29.0	-32.6	19.0	11.0
W49N	19 10 1.5	19 6 13.9	-33.6	11.9	8.0
W51(IRS2)	19 23 39.9	14 31 8.1	16.5	65.3	59.0
W51(Main)	19 23 43.9	14 30 36.4	12.5	61.3	55.0

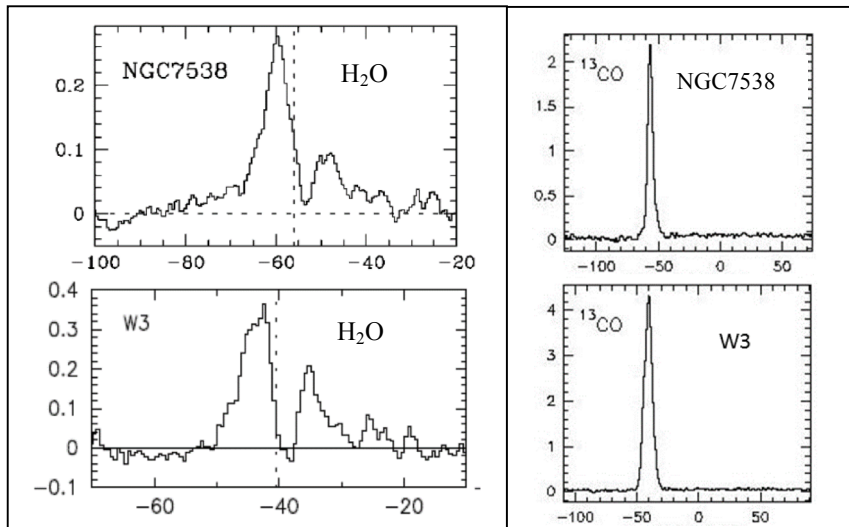
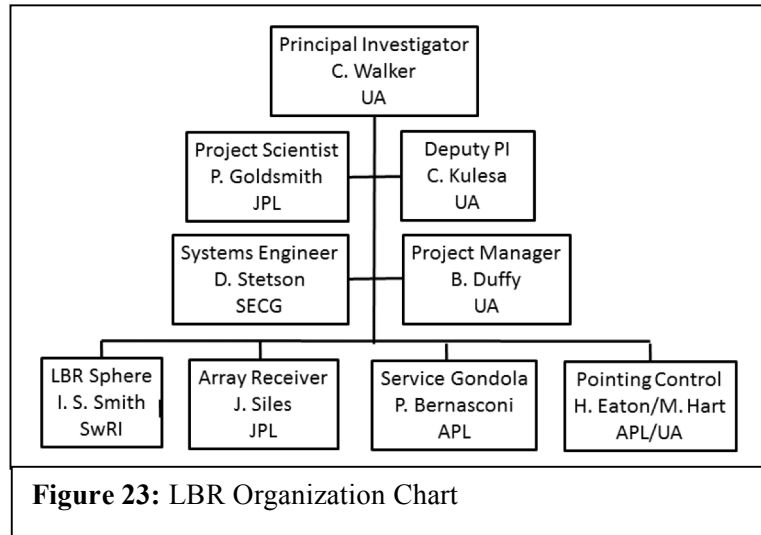


**Figure 22:** SWAS spectra of the 557 GHz H<sub>2</sub>O line (left) and  $^{13}\text{CO}$  J=5-4 (right) toward NGC7538 and W3 (Ashby et al. 2000; Snell et al. 2000).

### 3. Project Management

The LBR organizational structure is shown in Figure 23. Dr. Chris Walker (PI) is responsible for all aspects of the success and scientific integrity of LBR. He will be assisted at the University of Arizona by Dr. Craig Kulesa, who will serve as Deputy PI, and Brian Duffy, Project Manager (PM). The LBR science team will be led by Dr. Paul Goldsmith, who is the LBR Project Scientist (PS). The Instrument Team will be led by the DPI (Kulesa). Mr. I. Steve Smith (SwRI) will oversee the design and fabrication of the LBR



sphere. Dr. Bernasconi (APL) will oversee the LBR service gondola efforts and Dr. Jose Siles (JPL) will oversee the array receiver integration and testing. The master schedule shown in Figure 24 identifies the project's major milestones and development activities. The project as proposed can be completed in 3 years. However, if programmatic constraints are better met by spreading the effort over 4 years, this can be accommodated within the proposed cost envelope.

The LBR work plan is divided into a payload development program and an integrated testing program which serves to validate and verify the flight system repeatedly at the individual component, subsystem, and integrated payload levels. The testing program begins immediately at the component level, in parallel with payload development, so that issues can be solved early in the program cycle. The testing program culminates in an integrated thermal-vacuum test of the LBR Instrument Module and pointing system, which provides validation that data acquisition will perform optimally in flight. These tests will be coordinated by the PI/DPI and the individual payload subsystem leads. The instrument and science teams will make extensive use of electronic communication and management tools including e-mail, secure websites, on-line meetings and video communications to expedite accurate information dissemination. All management and control information will be posted on a secure LBR website maintained by the UA.

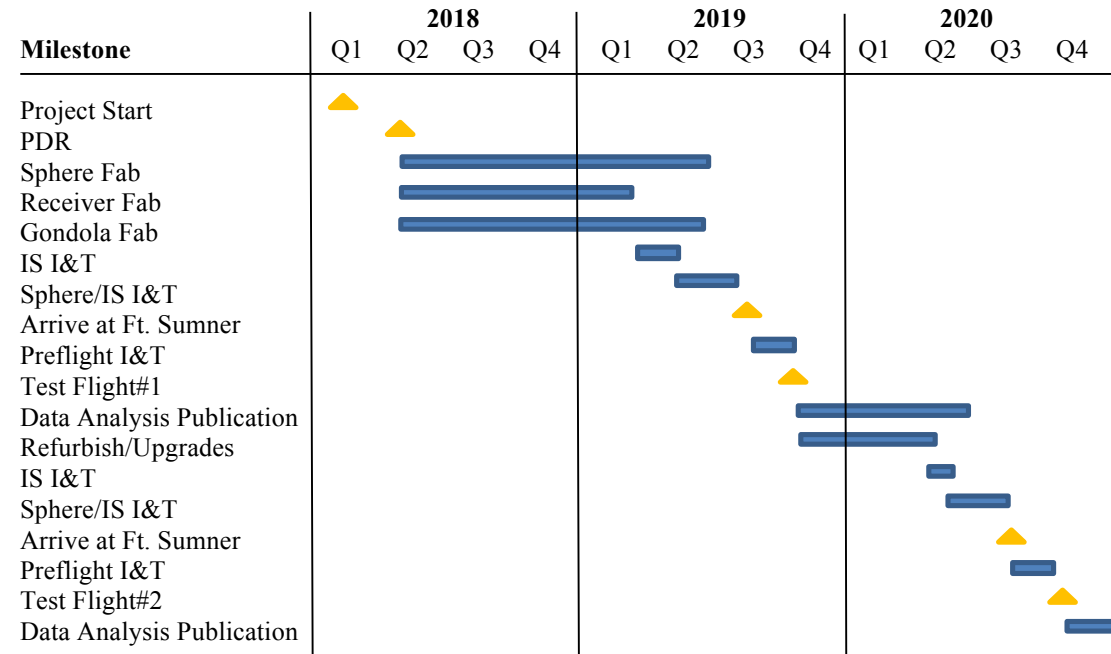
### 4. Dissemination of Results

As soon as data products are received and reduced they will be released to the public via the data archive on the LBR project web site. The data pipeline software, documentation, and associated parameters will also be archived allowing for a fully documented dataset of maximum utility for other members of the community. In addition, the data products will be made available at the Harvard Libraries Dataverse.

### 5. Future Plans

If these proposed North American test flights are successful, we will propose for an Antarctic LDB flight in the austral summer of 2021.

**Figure 24: LBR Project Schedule**



Note: Internal Quarterly Reviews will be held to review progress and plans, and status and issues will be reported to NASA following each review. NASA representatives will be welcome to attend any or all reviews and be present at key tests.

## B. References

- Ashby M., Bergin E., Plume R. and 18 others, 2000**, “ An Analysis of Water Line Profiles in Star Formation Regions Observed by the Submillimeter Wave Astronomical Satellite”, *Ap.J.*, 539, L115.
- Burge J., Benjamin S., Dubin M., Manuel A., Novak M., Oh C. J., Valente M., Zhao C., Booth J., Good J., Hill G., Lee, H., MacQueen P., Rafal M., Savage R., Smith M., and Vattiat B., 2010**, ”Development of a wide field spherical aberration corrector for the Hobby Eberly Telescope”, *Proc. of SPIE*, Vol. 7773, 77331J.
- Cadogan D. and Scarborough S., 2001**, “Rigidizable Materials for use in Gossamer Space Inflatable Structures”, *AIAA Gossamer Spacecraft Forum*, April 16-19, 2001, Seattle, WA.
- Elder D., 1995**, “Out from Behind the Eight-Ball: A History of Project Echo.”, *AAS History Series 16*. Univelt for the American Astronomical Society. ISBN 0-87703-388-9.
- Gordon W. E., and L. M. Lalonde, 1961**, “The Design and capabilities of an ionospheric radar probe”, *IRE Trans. Ant. Prop.* AP-9, No.1, 17-22.
- Hart M., Jefferies, S., Murphy N., 2016**, “Day Operation of a Sodium Guide Star”, *Proc. Of SPIE*, Vol. 9909, 99095N-2
- Kulesa C., 2011**, “Terahertz spectroscopy for astronomy: From comets to cosmology”, *IEEE Trans.Terahertz Sci. Technol.*, 1(1), 232.
- Küppers M., O’Rourke L., Bockelée-Moran, D. et al., 2014**, “Localized sources of water vapour on the dwarf planet (1) Ceres”, *Nature*, 505, 525.
- Melnick G. J., 1988**, “On the road to the large deployable reflector (LDR): The utility of balloon-borne platforms for far-infrared and submillimeter spectroscopy”, *Int. J. Infrared Milli. Waves*, 9(9) 781.
- Neufeld D. A., González-Alfonso E., Melnick G. et al., 2011**, “The widespread occurrence of water vapor in the circumstellar envelopes of carbon-rich asymptotic giant branch stars: First results from a survey with herchel/HIFI”, *Ap. J.*, 727, L29.
- Neufeld D. A., Stauffe, J. R., Bergin E. A. et al., 2000**, Submillimeter wave astronomy satellite observations of water vapor toward comet C/1999 H1 (Lee), *Ap. J.*, 539, L151.
- Snell R., Howe, J., Ashby M., and 15 others, 2000**, “ Water Abundance in Molecular Clouds”, *Ap. J.* 539, L101.
- Stacey G., J., 2011**, “THz Low Resolution Spectroscopy for Astronomy”, *IEEE Trans.Terahertz Sci. Technol.*, 1(1), 241.



**Walker C. K. et al., 2014**, “10 Meter Sub-Orbital Large Balloon Reflector,” 39th Int. Conf. on Infrared, Millimeter, and THz Waves, September 14-19, 2014, Tucson, AZ, <http://www.irmmw-thz2014.org/>.

**Walker C. K., 2015**, *TeraHertz Astronomy*, CRC Press, Taylor & Francis Group, Boca Raton, FL.

**Zerbini S. 1980**, “Direct solar and earth-albedo radiation pressure effects on the orbit of Pageos 1”, *Celestial Mechanics*, vol. 22, Nov. 1980, p. 307-334.

## F. Table of Personnel Roles, Responsibilities, and Relevant Experience

<b>Team Member</b>	<b>Role and Responsibility</b>	<b>Relevant Experience</b>
Chris Walker (UA)	Principal Investigator	THz Instrumentation, Star Formation, PI-STO
Craig Kulesa (UA)	Deputy PI, Instrument Scientist	THz Instrumentation, ISM Physics, PI-HEAT
Paul Goldsmith (JPL)	Project Scientist	THz Instrumentation, ISM Physics, PS-STO, US PS-Herschel
Steve Smith (SwRI)	LBR Sphere Lead	Expert in Inflatable Technology, former Chief of Balloon Project Office NASA
Gary Melnick (SAO)	D-PS, Ground Data System Lead	SWAS PI, ISM Physics and Chemistry
Pietro Bernasconi (APL)	Gondola Lead, IR Pointing System	STO-2, BOPPS, BRISSON, Gondola Lead
Michael Hart (UA)	Sodium Guide Star Lead	Adaptive Optics Expertise
Jose Siles (JPL)	Receiver Scientist	THz Receivers, STO Instrument Team
Chris Groppi (ASU)	Deputy Instrument Scientist	THz Instrumentation, ISM Physics
Doug Stetson (SSECG)	Systems Engineer	Light Sail PM, Innovative Mission and Systems Concepts
Brian Duffy (UA)	Project Manager	STO PM